Open Ceramics 8 (2021) 100183

Contents lists available at ScienceDirect

Open Ceramics

journal homepage: www.sciencedirect.com/journal/open-ceramics

Gel casting of silicon nitride foams using biopolymers as gelling agents

E. Guzi de Moraes [a,d,*], M.D.M. Innocentini [b], L. Biasetto [c], A.P. Novaes de Oliveira [d], D. Hotza [e], P. Colombo [a]

[a] Dipartimento di Ingegneria Industriale, University of Padova, Via Marzolo 9, 35131, Padova, Italy
[b] Course of Chemical Engineering, University of Ribeirão Preto, UNAERP, Ribeirão Preto, SP, 14096-900, Brazil
[c] Dipartimento di Tecnica e Gestione dei Sistemi Industriali, University of Padova, Stradella San Nicola 3, 36100, Vicenza, Italy
[d] Graduate Program in Materials Science and Engineering (PGMAT), Department of Mechanical Engineering (EMC), Laboratory of Glass-Ceramic Materials (VITROCER), Federal University of Santa Catarina (UFSC), 88040-900, Florianópolis, SC, Brazil
[e] Department of Chemical Engineering (EQA), Laboratory of Ceramics Processing (PROCER), Federal University of Santa Catarina (UFSC), 88040-900, Florianópolis, SC, Brazil

ARTICLE INFO

Keywords:
Silicon nitride foams
Gel casting
Biopolymers

ABSTRACT

Si_3N_4-based foams were prepared by the gel casting route using egg-albumen, agar-agar, or methylcellulose as biopolymer gelling agents. Microstructural, permeability, and mechanical properties of the foams were determined. The use of a variety of environmentally friendly gelling agents produced Si_3N_4 foams with a wide range of porosity (79–89%), mean cell size (199–852 μm), and mean window size (51–152 μm). The pressureless sintering method was successfully applied and resulted in Si_3N_4 foams with compressive strengths ranging from 1.6 to 9.4 MPa when treated at 1600 °C and up to 33.5 MPa when sintered at 1700 °C, due to the formation of the β–Si_3N_4 phase. Darcian (k_1) and non-Darcian (k_2) permeability coefficients were 4.41×10^{-12} to 1.61×10^{-10} m^2 and 5.07×10^{-7} to 1.02×10^{-6} m, respectively, allowing the produced Si_3N_4 foams to be used in a wide variety of fluid flow and filtering applications.

1. Introduction

Cellular ceramics are highly porous and lightweight materials tailored to possess an exceptional combination of functional properties, such as low thermal conductivity, high-temperature stability, and excellent thermal shock resistance, good resistance against crack propagation, high permeability, and high surface area [1–5]. These properties are directly related to their interconnected pore network (pore size distribution and porosity at multiple scales), which is a consequence of the processing route selected to design their structure. Among a wide-ranging of conventional technologies, including the use of replica [6,7], sacrificial templates [8], direct foaming (emulsion [9] and foam [10] templating), it is interesting to highlight the gel casting method [11,12], which is near-net-shape processing that allows obtaining reliable, complex-shaped and high-strength porous ceramic bodies.

Gel casting technology is based on the fast consolidation of a homogeneous suspension into a stiff solid-like body, or gel, employing *in situ* formation of a percolating network of ceramic particles through polymerization of monomers or thermogelation of biopolymers [13–15]. Gelling agents from the food industry, *e.g.*, gelatin, ovalbumin, and polysaccharides such as sucrose, agar-agar, carrageenan, starch, and cellulose, for instance, have been used to overcome the disadvantages of the toxicity of the monomers originally applied in gel casting processing route [3,12].

Silicon nitride (Si_3N_4) foams exhibiting a good combination of mechanical performance and thermal properties can be processed by direct foaming methods, such as preceramic polymers [16], particle-stabilized foams [17], emulsification based on surfactant stabilization [18], and gel casting [19,20], among others. Besides, these materials are used in a wide range of technological applications as aerosol filters, filtering membranes, catalyst substrates, thermal insulators, gas burner media, refractory coating, heat exchangers, and also as porous implants in the area of biomaterials [5,8,21].

Nevertheless, the sintering of silicon nitride-based ceramics requires high temperatures (>1800 °C) and generally is assisted by pressure, due to the strong covalent bonds between silicon and nitrogen and to the very slow solid-state diffusion rates [22]. The use of sintering additives can enhance the densification and sintering kinetics (sintering activity) and lower the sintering temperature by the formation of a eutectic liquid phase with the oxide surface layer present on the silicon nitride powder,

* Corresponding author. Dipartimento di Ingegneria Industriale, University of Padova, Via Marzolo 9, 35131, Padova, Italy.
E-mail address: e.g.guzi@posgrad.ufsc.br (E. Guzi de Moraes).

https://doi.org/10.1016/j.oceram.2021.100183
Received 26 July 2021; Accepted 12 August 2021
Available online 9 September 2021

promoting the solution-precipitation process, in which α–Si_3N_4 dissolve into the liquid phase and precipitate as β–Si_3N_4, known as the α→β phase transformation [23–25]. Lowering the sintering temperature while keeping the microstructure and mechanical properties is therefore not only a technological challenge but also an economic goal since the processing costs of complex parts of nitride-based ceramics can be proportionally reduced [26].

The current work is concerned with the fabrication of silicon nitride foams with tailored microstructure in terms of porosity (>75 vol%) and cell size distribution (>150 μm) using a gel casting processing method associated with the aeration of an aqueous suspension and environmentally friendly biopolymers as gelling agents. Alternative biopolymers such as agar-agar [12], globular proteins (egg white albumen) [13,20], and methylcellulose [14,27] were used to produce silicon nitride foams in a wide range of cell and window sizes and porosities aiming at a broader range of fluid flow and thermal applications.

The microstructure, mechanical properties, and permeability of the gel casting Si_3N_4 foams pressureless sintered were evaluated. Additionally, the influence of the sintering additives, Y_2O_3 and MgO on the solution-reprecipitation process (α→β phase transformation), and the effect of the temperature on the morphology of the elongated β–phase was investigated.

2. Experimental

2.1. Powder raw materials and additives

Egg white albumen (90.5% of Ovalbumin, AppliChem GmbH, Darmstadt, Germany), average molecular weight Mw = ~45,000, was used as gelling additive in powder form.

Agar-agar (Erbamea S.R.L, Italy) was used as a gelling additive. Aqueous agar solutions at 3 wt% (1 wt% of agar powder based on the Si_3N_4 powder suspension content) were prepared in a flask by mixing the gel-former with deionized water heated up to 90 °C during 120 min [12,14].

Water-soluble methylcellulose (MC, Methocel™ A4M, Dow Chemical Company, Italy) was used as a gelling additive. Methylcellulose solutions at 0.5 wt% were prepared in a flask containing deionized water heated up to 90 °C followed by the addition of the gel-former and subsequent magnetic stirring during 120 min. Afterward, the solution was cooled to room temperature in continuous mixing [27].

A detailed procedure for suspension preparation can be found elsewhere [28], with a complete description of ceramic powders used in this study (Table 1). A commercial Si_3N_4 powder (~91.5% of α-phase) containing Fe impurities (100 ppm), and 5 wt% Y_2O_3 and 5 wt% MgO as sintering additives (Labeled as SN-5YM), were used for the feedstock preparation. Powder batches were wet-milled in ethanol for 4 h, using silicon nitride cylinders and planetary velocity of 300 rpm. The slurry was dried, sieved through a 300 μm screen, and then the powder mixture was treated at 600 C for 2 h. The controlled preoxidation of the silicon nitride powder surface could improve significantly their aqueous dispersibility, thus decreasing the viscosity of the suspension [29].

Table 1
Ceramic powder characteristics.

Powder	Purity (%)	Particle size, d_{50} (μm)	Supplier
α-Si₃N₄	>96	1.95	Yantai Tomley Hi-tech New Materials, Shandong, China
Y₂O₃	>99.95	0.05	Inframat Advanced Materials L.L.C., Manchester, USA
MgO	>99.99	4.6	Bitossi Ceramiche S.R.L., Montelupo Fiorentino, Italy

2.2. Foam processing and sintering

The solids loading of aqueous Si_3N_4 colloidal suspensions varied according to the gelling agent and thermal gelling procedure used. In the case of egg white albumen, the water-based Si_3N_4 slurries with 30 vol% of solids (labeled as SN-5YM30), and containing 1 wt% of polyacrylic acid, PAA, (based on the ceramic powder content) were prepared by step-wise adding the dry powder to deionized water upon continuous stirring with a laboratory mixer. The ceramic suspension was homogenized by ball milling for 2 h at 200 rpm using Si_3N_4 cylinders. In the case of Si_3N_4 suspensions, the pH was set to values above 11.4 by adding small aliquots of NaOH, 0.1 N. Afterward, the slurry was aerated with a double shear mixer (in a household mixer Silvercrest SHM 300 A1, at full power), during 2 min followed by the addition of 5 wt% of albumen (egg white, based on the ceramic powder content) and subsequently, the suspension was vigorously stirred during 5 min to foaming. Then, the foams were poured in a Teflon mold and thermal gelling occurred in a dryer at 80 °C for 2 h to cross-linking of amino acids (cistein), and at ambient air for approximately 24 h. Thermal treatment was conducted in two steps: i) pre-calcination at 650 °C (2 h; 1 °C/min heating rate) to decompose the organic phase; ii) sintering at 1600 °C (3 h, 2 °C/min heating rate) under 99.99% N_2 flow [18].

For agar, the incorporation of the solution (maintained at 60 °C) required the previous heating of the Si_3N_4 suspension with 35 vol% of solids, at a temperature above 60 °C, to equalize the system temperature to avoiding early gelation of the solution.

After adding the agar solution, the final Si_3N_4 suspension concentration reached 30 vol% (~59 wt%). Since the gel casting suspensions containing agar solution and Si_3N_4 suspension were mixed, 1.0 wt% of Tergitol TMN–10 (based on the ceramic powder content), a non-ionic surfactant, was incorporated into the hot suspension. Thereafter, the gel casting suspensions were mechanical stirred (in a household mixer Silvercrest SHM 300 A1, at full power) with a double shear mixer for 10 min to promote bubble formation [12]. The foams were poured into a plastic mold and cooled down at 15 °C using cold water to promote gel-network formation. The foams were dried at ambient air for approximately 24 h. The heat treatment of the consolidated foams was performed in two steps as earlier reported for egg white albumen foams.

Particularly for methylcellulose (MC), gel casting suspensions were prepared by step-wise addition of 30 or 35 vol% of Si_3N_4 particles in a previously prepared solution of methylcellulose, instead of water, containing 1 wt% PAA (based on the ceramic powder content), followed by homogenization with ball milling for 2 h, as earlier described for egg white albumen suspension preparation. Thus, a non-ionic surfactant, Tergitol TMN–10 (1.0 wt%, based on the ceramic powder content) was incorporated in a gel casting suspension by stirring (in a household mixer Silvercrest SHM 300 A1, at full power) with a double shear mixer for 10 min for foaming. The foams were poured into a silicon mold and kept at ~47 °C overnight to form a gel network and dried at ambient air for 24 h. In the case of MC foams, thermal treatment was conducted at the same conditions described above for egg white albumen foams (1600 °C), or alternatively at high sintering temperatures (1700 °C), to evaluate the β–Si_3N_4 phase evolution.

2.3. Characterization

The crystalline phases were determined on powdered samples by X-ray diffractometry using a Bruker AXS D8 Advance diffractometer (CuKα, 40 kV, 40 mA, 0.05°, 2s). The data were analyzed utilizing the ICSD database, and the weight fractions of the α– and β–Si_3N_4 crystalline phases were evaluated by the method described in [30]. The microstructure of the Si_3N_4 based foams was investigated by scanning electron microscopy (FEI Quanta 200, FEI Italia, Milan, Italy). Cell size and cell windows sizes were measured by the linear intercept method (ASTM E112-12), using an image analysis program (Axio Vision LE). The average values were obtained considering stereological relations (ASTM

D3576-98), the relationship between the average measured chord length t and the average pore diameter D is D = t·1.623. The aspect ratio of the rod-like β–Si_3N_4, based on length-to-diameter ratio, was also measured from SEM images, considering the average of 10% of the crystals with the highest aspect ratio. Due to the difficulty in accurately determine the true length of the random-oriented interlocking crystals, the total length was measured from intercept to intercept.

The total porosity was calculated from the weight-to-volume ratio of the samples. The cellular microstructures of the sintered Si_3N_4 foams prepared using different gel formers were compared in terms of porosity considering an array of uniform cell diameters. The open porosity (V_P) of cellular ceramics ($0.7 < V_P < 1.0$) was calculated according to Equation (2), where $k = d/D$; cell window (d) and cell size (D) [31].

$$V_p = \frac{\pi}{\sqrt{2}}\left[\frac{3}{1-k^2} - \frac{5}{3}\left(\frac{1}{1-k^{-2}}\right)^{3} - 1\right] \quad (1)$$

The mechanical behavior of the Si_3N_4 based foams was determined by uniaxial compression strength tests performed using a hydraulic mechanical testing machine (1121 UTM, Instron, Norwood, MA, USA), according to ASTM C133-97 standard. The cross-head speed was 1.0 mm/min and the compressive load cell was 5 kN. Specimens with a nominal size of 10 mm × 10 mm × 10 mm, cut from larger bodies, were tested for each sample. Each data point represents the average value of five individual tests.

The permeation behavior of the Si_3N_4-based foams was evaluated at room temperature by a laboratory-made apparatus, following the procedure described elsewhere [32–34]. The experimental pressure drop x gas velocity dataset was used to fit permeability coefficients according to Forchheimer's equation for compressible flow:

$$\frac{P_i^2 - P_o^2}{2PL} = \frac{\mu}{k_1}v_s + \frac{\rho}{k_2}v_s^2 \quad (2)$$

in which P_i and P_o are, respectively, the absolute gas pressures at the entrance and exit of the sample, v_s is the superficial gas velocity, determined by dividing the exiting volumetric flow rate Q, by the sample face area A exposed to flow, L (0.5–0.8 cm) is the sample's thickness, μ is the gas viscosity (1.77–2.20 × 10^{-5} Pa·s), and ρ is the gas density (1.15–1.68 kg/m^3), evaluated for the pressure P_o = 713–760 mmHg and T = 16–24 °C. The parameters k_1 (expressed in square meters) and k_2 (expressed in meters) are respectively known as Darcian and non-Darcian permeability coefficients, in reference to Darcy's law, which establishes a linear dependence between ΔP and v_s. These coefficients weigh the contributions of viscous and inertial losses on the total pressure drop, i.e., the influence of viscous and inertial interactions between fluid and the porous medium [35]. The great advantage of using coefficients k_1 and k_2 is that they do not depend on the type of fluid and the velocity applied, but they are instead intrinsically related to features of the porous structure, such as the morphology, size distribution, connectivity, and volume fraction of the voids available for fluid flow.

The first term of Forchheimer's equation, $(\mu/k_1)\cdot v_s$ represents viscous energy losses due to friction between fluid layers and prevails at low fluid velocities. On the other hand, the quadratic term, $(\rho/k_2)\cdot v_s^2$, which is not considered by Darcy's equation, becomes increasingly significant at higher velocities and represents the kinetic energy losses due to changes in the direction of motion and to acceleration or deceleration of the fluid caused by changes in the flow path (contraction or enlargement of the pore section or pore tortuosity along the flow direction) [35,36].

The experimental evaluation of permeability parameters was carried out with argon and air flow at room temperature in a laboratory-made gas permeameter described elsewhere [32]. Two to three disks of ~36 mm of diameter and ~7 mm of height were tested for each sample. The gas was forced to flow in a stationary regime through the cylindrical samples had their lateral surface previously sealed (using Teflon tape), to allow the gas flow to occur only in the top-bottom direction [35–37].

3. Results and discussion

3.1. Structural and microstructural characterization

The X-ray diffraction patterns of the as-prepared and sintered Si_3N_4 gel casting foams are reported in Fig. 1. The main phase was α–Si_3N_4 in all samples, and an increase in the β–phase was observed after sintering, from 12.9% for the as-prepared powders to about ~30% for sintered foams, as estimated based on the ratio of the intensities of the peak for both phases (located at 2θ = 35.4° for the alpha phase and at 2θ = 35.9° for the beta phase), using a normalizing factor to correct the peak intensities from errors due to extinction and preferred orientations [30]. The increase in β–Si_3N_4 during sintering in the presence of a liquid Y_2O_3–MgO-containing phase is owing to a solution-reprecipitation mechanism that starts occurring around 1600 °C and occurs preferentially at the contact areas between particles [23,38,39]. The peaks relative to the sintering aids disappeared after heating due to their incorporation into an amorphous intergranular phase [28,39–41].

The highly interconnected open-cell morphology of the SN-5YM30 sintered foams prepared using different gelling agents is shown in Fig. 2. A general view of albumen, agar, and methylcellulose gel cast foams is reported in Fig. 2 (a), **(c)**, and **(e)**, respectively. The high stability of the albumen wet foams was achieved by thermal gelling of the liquid phase at 80 °C allowing a narrower distribution in the average cell size (D_{10} = 121 μm, D_{50} = 199 μm, D_{90} = 278 μm), and window size (d_{10} = 22 μm, d_{50} = 51 μm, d_{90} = 75 μm). It is worth noting that these values are related to the adsorption of proteins at the air-water interface, where protein denaturation (i.e., a conformational change) and intermolecular cross-linking occur, forming a flexible and cohesive film inhibiting the variation in the size of the bubbles [42–44].

On the other hand, the thermal gelling of the liquid foam containing 1 wt% of agar-agar as a solution occurs during cooling at ~15 °C in a cold water bath. A statistical analysis of the data obtained from SEM images showed monomodal distribution of cell sizes around D_{10} = 302 μm, D_{50} = 456 μm, D_{90} = 798 μm, and window size around d_{10} = 45 μm, d_{50} = 79 μm, d_{90} = 160 μm. These values are much higher than that for egg white albumen foams owing to foaming ability and dynamic adsorption/desorption of surfactants leading to coalescence mechanism [12].

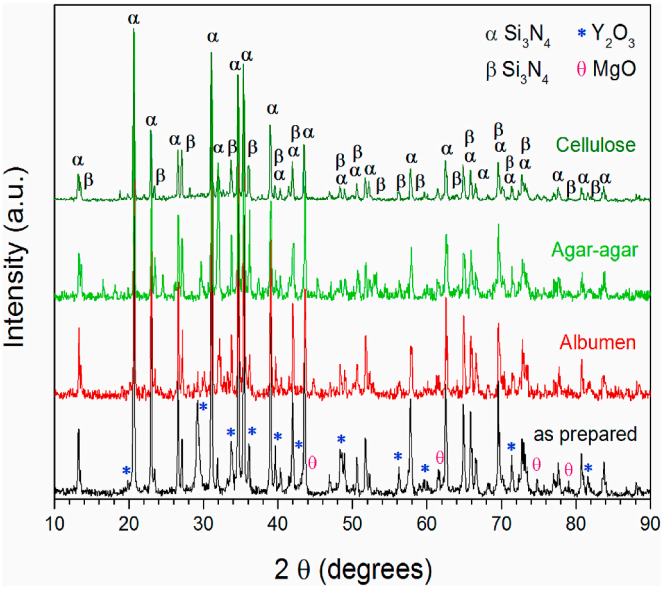

Fig. 1. XRD patterns of as-prepared and sintered (1600 °C) Si_3N_4 gel casting foams (egg white albumen, agar-agar, and methylcellulose (labeled as cellulose)) containing 5 wt% Y_2O_3 and 5 wt% MgO. (ICSD α–Si_3N_4 # 04–0360, β–Si_3N_4 # 033–1160, Y_2O_3 # 043–0661, MgO # 045–0946).

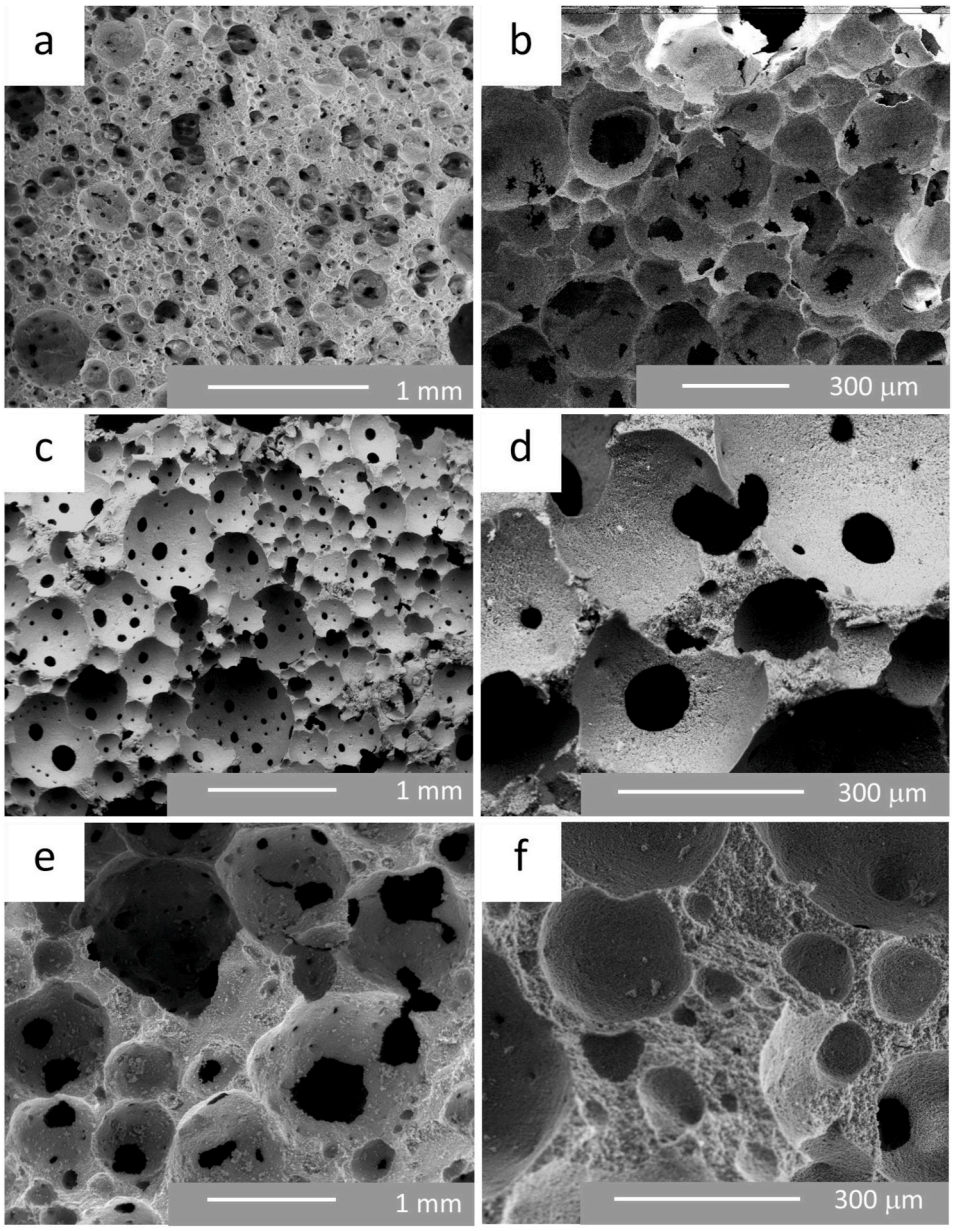

Fig. 2. SEM images of the fracture surface of SN-5YM30 sintered (1600 °C) gel casting foams prepared using different gelling agents: egg white albumen (a) and (b); agar-agar (c) and (d); and methylcellulose (e) and (f).

Table 2
Summary of the physical and mechanical properties of the Si_3N_4 foams from the gel casting process.

Si_3N_4 foams	*Cell size, D*[a] *(μm)*	*Cell window size, d (μm)*	*Total Porosity*[b] *(%)*	d/D	V_P[c] *(%)*	σ *Compressive strength (MPa)*
Conventional Pressureless Sintering 1600 °C, N_2 flow						
5 wt% Albumen	199 ± 14	51 ± 6	79.1 ± 1.2	0.256	81	9.4 ± 2.0
1 wt% Agar-agar	456 ± 47	79 ± 18	86.1 ± 0.9	0.173	77	5.0 ± 1.1
30 vol% Methylcellulose	852 ± 89	152 ± 36	89.3 ± 0.5	0.222	79	1.6 ± 0.5
35 vol% Methylcellulose	643 ± 69	109 ± 32	83.0 ± 1.1	0.169	77	7.5 ± 2.1
Average Linear Shrinkage (%)	~14					
Conventional Pressureless Sintering 1700 °C, Static N_2						
30 vol% Methylcellulose	773 ± 88	152 ± 30	81.4 ± 0.5	0.183	77	8.1 ± 1.0
35 vol% Methylcellulose	544 ± 35	108 ± 8	72.0 ± 1.0	0.159	76	33.5 ± 3.9
Average Linear Shrinkage (%)	~16					

[a] Cumulative cell size and cell window size distribution, *D* (average cell size, d_{50}) and *d* (average cell window size, d_{50}), respectively, measured from SEM images using linear intercept method.
[b] Calculated by assuming that the theoretical density of Si_3N_4 ceramic is 3.2 g·cm^{-3}.
[c] Open porosity, V_P, calculated from Eq. (2).

In addition, methylcellulose (MC) foams exhibited similar spherical interconnected morphology to the samples processed using agar; nevertheless, the thermal gelation occurred with heating at ~47 °C, as a result of the syneresis mechanism [14]. A wide distribution was achieved for cell sizes (D_{10} = 408 μm, D_{50} = 852 μm, D_{90} = 1360 μm), and for window size (d_{10} = 65 μm, d_{50} = 152 μm, d_{90} = 355 μm). Depending on the adsorption behavior of MC at the air-water interface, which is diffusion-controlled, coalescence of the newly formed bubbles can take place [3,45–47].

Fig. 2 shows the strut structure featuring dense packing of particles, residual porosity, and some cracks at higher magnification images (Fig. 2 (b), **(d)** and **(f)**, 200x magnification). The average cell size and cell window size, the total porosity, and the mechanical strength values of Si_3N_4 sintered foams are summarized in Table 2.

With the increase of the solids content to 35 vol% of Si_3N_4-based powder concentration, the methylcellulose foams displayed a similar interconnected network of cells morphology; however, a strong packing of particles was observed on cell walls and struts (Fig. 3), which slightly influenced the average cell size (D_{50} = 643 μm), window size (d_{50} = 119 μm), and porosity, which decreased ~7% (Table 2).

The effect of increasing the sintering temperature to 1700 °C on the microstructure and α→β transformation was also investigated. The X-ray diffraction patterns of the methylcellulose foams prepared with 35 vol% of solids concentration are reported in Fig. 4.

The amount of β–phase significantly increased up to ~98% (estimated value [30]), since the rate of the solution-precipitation process increased with sintering temperature, enabling the formation of elongated β–Si_3N_4 crystals [47].

At high temperatures, the low-temperature phases dissolved in the silicate liquid phase, α–Si_3N_4 transforms into metastable SiN_4 tetrahedra and finally into thermodynamically stable β–Si_3N_4. The overall α→β transformation depends on the chemical composition of the liquid phase [39]. As discussed earlier, the peaks related to the sintering aids disappeared suggesting their incorporation into the intergranular oxynitride phase [28,39–41].

Pyzik and Beaman [39] studied the combined effect of different ratios of Y_2O_3:MgO on the microstructure (β–grains) and mechanical properties (strength and fracture toughness) of hot-pressed (1825 °C) silicon nitride dense components. The microstructure of the composition Si_3N_4 + 7.5 wt% Y_2O_3 + 7.5 wt% MgO consists of large and small elongated grains with improved mechanical properties: 5.9 MPa $m^{1/2}$ of fracture toughness and 650 MPa of flexure strength. Since low-viscosity glass (MgO) provides rapid mass transport, leading to a coarse β–Si_3N_4, while high-viscosity glass (Y_2O_3), slow mass transport causes a reduction in the rate of grain growth, leading to refined β–Si_3N_4 [39].

On the other hand, pressureless sintered dense Si_3N_4 containing different ratios of Y_2O_3 from 1 to 6 wt% concerning 5 wt% of MgO were

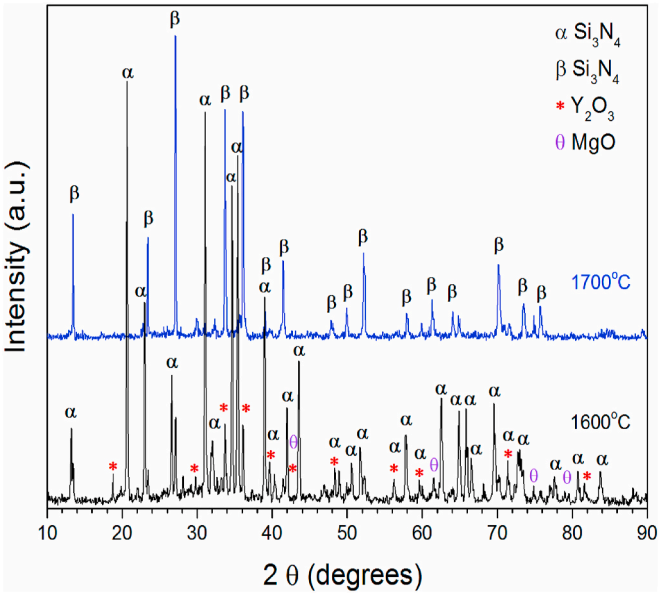

Fig. 4. XRD patterns of SN-5YM35 methylcellulose foams containing 5 wt% Y_2O_3 and 5 wt% MgO. (ICSD α–Si_3N_4 # 041–0360, β–Si_3N_4 # 033–1160, Y_2O_3 # 043–0661, MgO # 045–0946).

investigated by Ling and Yang. The combination of Y_2O_3 and MgO as sintering additives is very effective for the densification of silicon nitride. The optimized composition 4 wt% Y_2O_3 + 5 wt% MgO achieved 99% of relative density, and improved mechanical properties: 7.5 MPa $m^{1/2}$ and 950 MPa of bending strength [22].

Fig. 5 presents SEM images of the Si_3N_4 methylcellulose foams prepared with 30 and 35 vol% of solids concentration and sintered at high temperatures. Gel casting foams featured a similar interconnected network of spherical cell morphology and presenting typical rod-like β–Si_3N_4 crystals. When the sintering temperature was increased to 1700 °C, the porosity of the SN-5YM30 methylcellulose foams decreased from 89 to 81 vol%, since the α→β transformation takes place without much densification [38]. In addition, the average cell size slightly decreased with the sintering temperature, as given in Table 2. A similar influence of the temperature was observed on the porosity of the SN-5YM35 methylcellulose foams, which decreased from 83 to 72 vol%. Note also the presence of a wide distribution of cell sizes of D_{10} = 387 μm, D_{50} = 544 μm and D_{90} = 718 μm (Table 2). A general view of the interlocking of β–Si_3N_4 present on cell walls and struts of the SN-5YM30 methylcellulose foams is reported in Fig. 5 (a), and in Fig. 5 (b) with higher magnification of β–crystals, which exhibit an aspect ratio around

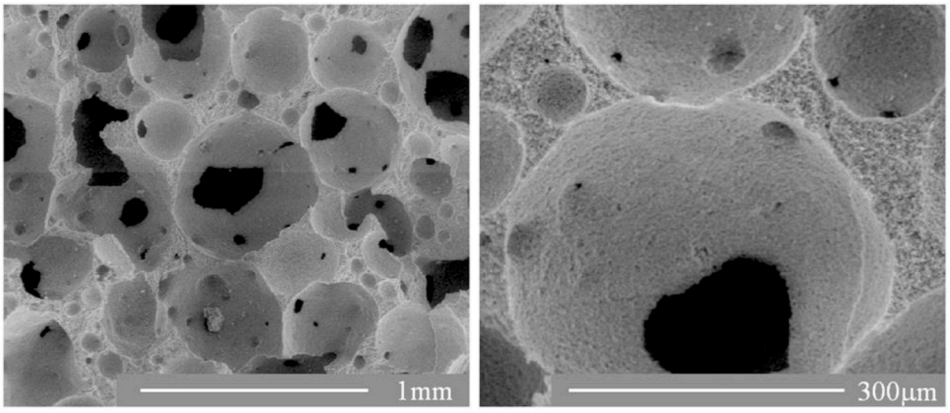

Fig. 3. SEM images of the fracture surface of SN-5YM35 sintered (1600 °C) methylcellulose foams: a) general view and b) higher magnification, detail of a dense packing of particles on cell walls and struts.

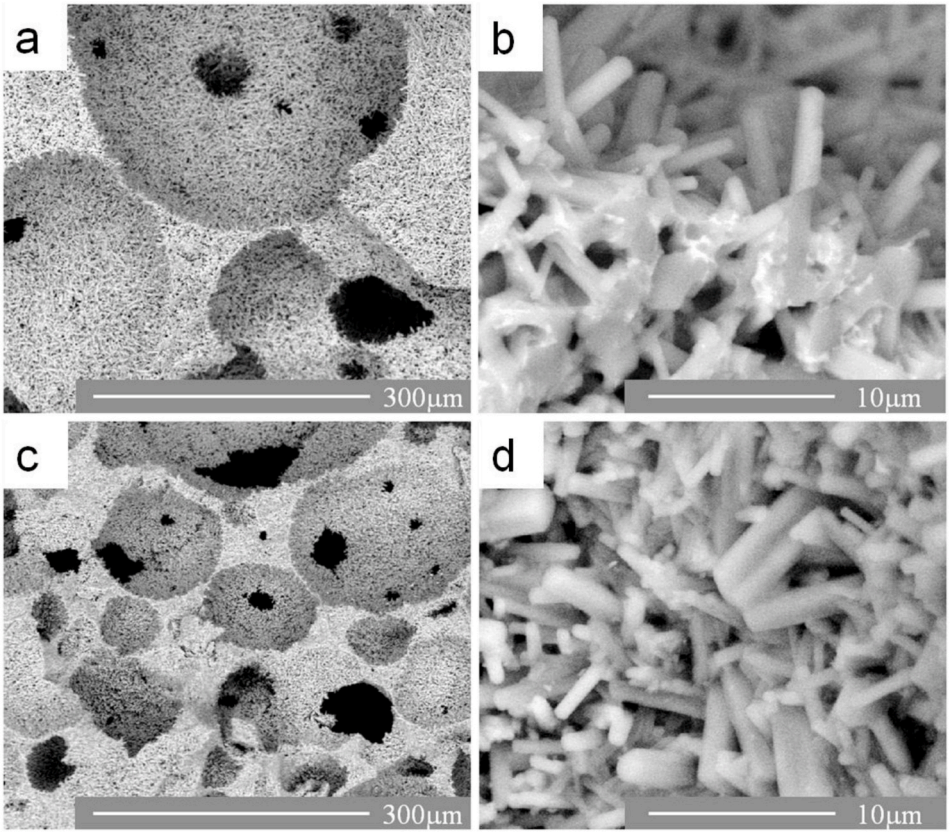

Fig. 5. SEM images of the fracture surface of Si_3N_4 + 5 YM sintered (1700 °C) methylcellulose foams: 30 vol% of solid concentration a) general feature and b) higher magnification (detail of interlocking β–crystals); 35 vol% of solid concentration c) general view and d) higher magnification (detail of interlocking β–crystals).

~7.0 ± 0.9. On the other hand, a slight decrease in aspect ratio (~6.0 ± 2.0) is observed for SN-5YM35 methylcellulose foams, as seen in Fig. 5 (c) and (d). The aspect ratio slightly decreased with the solid concentration, as the anisotropic growth of β–Si_3N_4 crystals became restrained when the porosity decreased [47]. Therefore, the rate of α→β transformation was increased with the heat treatment temperature, which enabled the solution of α–Si_3N_4 into the amorphous liquid Y_2O_3–MgO-containing phase and subsequently precipitation of β–Si_3N_4 (less soluble and more stable) resulting in the formation of elongated interlocking β–crystals [48].

3.2. Porosity and mechanical behavior

The calculated open porosity values (V_P) showed differences with the values obtained from the weight-to-volume ratio for all gel casting foams, as seen in Table 2.

The destabilization mechanisms such as coalescence (association of neighboring air-bubbles) and Ostwald ripening (diffusion of air-molecules from smaller to larger bubbles over time) [3] likely occurred, allowing a wide distribution of cells and windows sizes, thus the model was not entirely representative [31]. Permeability and mechanical strength parameters are also very dependent on the pore size and porosity [49,50].

Compressive strength as a function of total porosity is reported in Fig. 6 for gel casting foams produced with different gelling agents and containing 30 or 35 vol% of solids concentration. The values increased from 1.6 to 9.4 MPa, when porosity decreased from 89 to 79 vol% (Table 2). Higher values of strength are associated with egg white albumen, which is more efficient to stabilize the foam. According to Clark et al. [43], during surface denaturation, the interaction between neighboring molecules enables the formation of a cohesive viscoelastic surface layer of uniform thickness that makes desorption of proteins

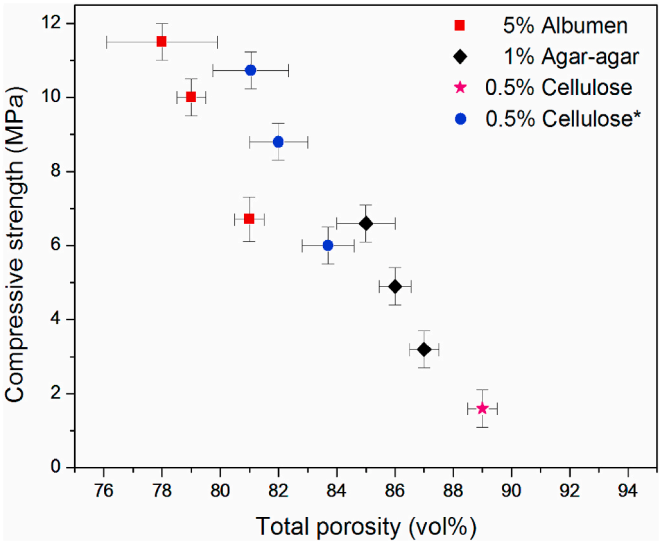

Fig. 6. Compressive strength as a function of total porosity for sintered (1600 °C) SN-5YM30 gel casting foams based on egg white albumen, agar-agar, and methylcellulose (labeled as Cellulose). Foam prepared with methylcellulose with 35% solids concentration was labeled as Cellulose*.

molecules highly improbable. On the other hand, agar-agar and methylcellulose gel cast foams exhibit lower compressive strength values, as a result of higher porosity (>85%) and larger cells and windows sizes, which impact the thickness of the struts compromising the structural integrity of the foam [51].

In addition, varying the solids concentration of methylcellulose

foams (labeled as cellulose*) to 35 vol%, we observed an increase in the compressive strength 7.5 MPa (Table 2), due to the decrease in porosity and dense packing of Si_3N_4 particles on the cell walls and struts. The variation in density and strength among samples processed using different gel formers reflects the differences between thermal gelling and indeed leads to the design of a wide range of microstructures concerning cell and windows sizes and porosity.

The development of ~98% beta-Si_3N_4 elongated rod-like crystals caused by sintering at 1700 °C, as already outlined, clearly influenced the strength employing increased degree of bonding between grains, since with increasing sintering temperature diffusion is enhanced, as well as the toughness mechanisms of grain bridging and pullout. A significant increase in the compressive strength values was obtained for SN-5YM30 methylcellulose foams from 1.6 to about 8.1 MPa, with the increase of the sintering temperature to 1700 °C. Similarly, higher values were achieved for foams prepared with 35 vol% of solids concentration, 7.5–33.5 MPa (Table 2), which indicates that fine-sized, fibrous Si_3N_4 crystals favored high strength in porous Si_3N_4 ceramics [52].

3.3. Permeability

Fig. 7 shows a comprehensive permeability map that classifies porous structures according to their morphology or application. The map is based on hundreds of k_1 and k_2 values from the literature. The position in the graph of the data from this study (k_1 from 4.41×10^{-12} to 1.61×10^{-10} m^2 and k_2 from 5.07×10^{-7} to 1.02×10^{-6} m, Table 3) indicates that the use of different gel formers (albumen, agar-agar, and methylcellulose) allowed the processing of Si_3N_4 foams with a broad range of permeability, included in the classes of gel casting foams, granular and fibrous filters. Indeed, agar foams present larger channels than those present in albumen foams. Also, tortuosity that arises from cell-size variation can affect the permeability coefficients k_1 and k_2 *e.g.*, if the cell sizes of the foam are constant, permeability is well correlated to porosity [53].

Table 3
Summary of permeability coefficients k_1 and k_2 obtained by fitting of Forchheimer's Equation for the Si_3N_4 foams from the gel casting process.

Si_3N_4 gel casting foams		
Gel former (sintering temperature)	k_1 (m^2)	k_2 (m)
Egg white albumen (1600 °C)	4.41×10^{-12}	4.01×10^{-7}
Agar-agar (1600 °C)	3.30×10^{-12}	1.02×10^{-6}
30 vol% Methylcellulose (1700 °C)	1.61×10^{-10}	2.58×10^{-6}

4. Conclusions

Gel casting of highly interconnected and permeable Si_3N_4 ceramic foams was studied in this work using egg white albumen, agar-agar, or methylcellulose biopolymers as gelling agents. A pressureless sintering method with additions of MgO and Y_2O_3 was successfully employed to reduce the complexity and costs of the manufacturing process. Total porosities of sintered bodies ranged from 79.1 to 89.3 vol%, with a wide

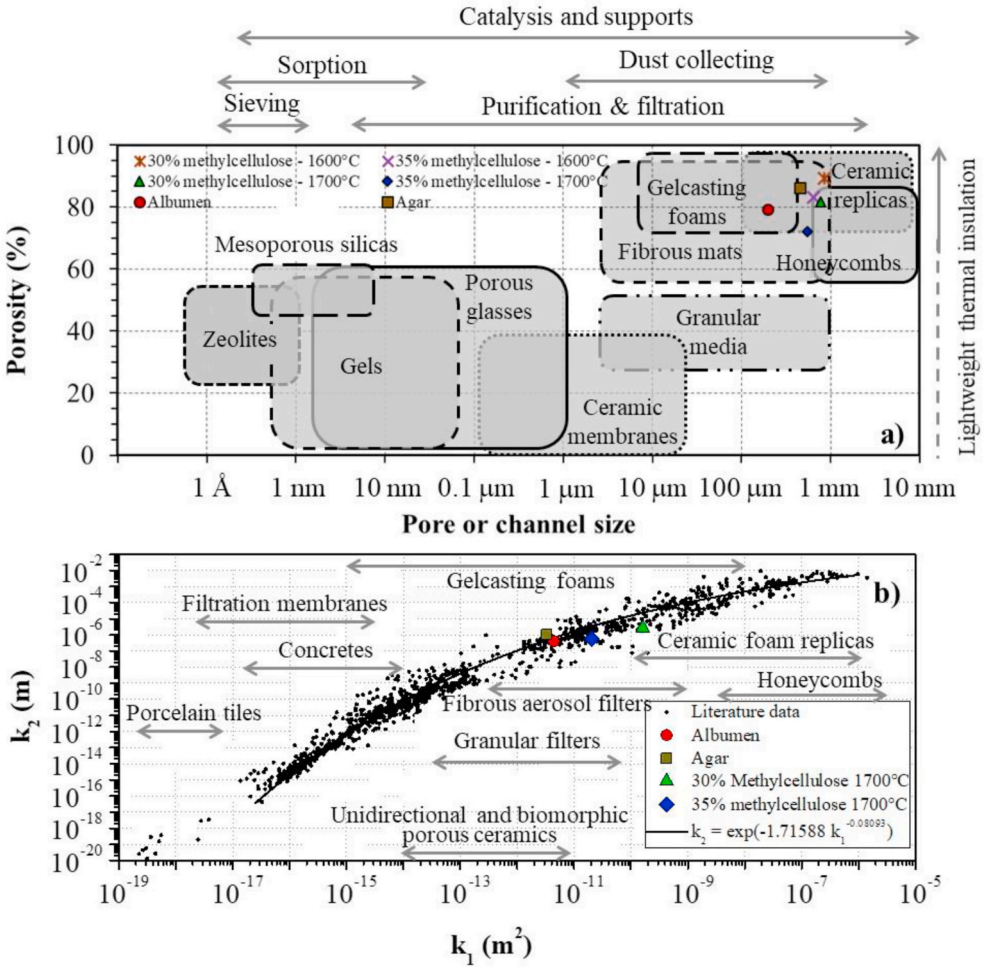

Fig. 7. Classification of porous materials according to their (a) porosity; (b) permeability coefficients, with the location of Si_3N_4 sintered (1600 °C) gel casting foams based on egg white albumen and agar-agar, as well sintered (1700 °C) gel casting foams based on methylcellulose tested in this work. (Adapted from [54,55]).

range of cells and windows sizes. Compressive strength varied from 1.6 to 9.4 MPa for sintering at 1600 °C to 8.1–33.5 MPa at 1700 °C, with methylcellulose foams based on 30 or 35% solids concentration. The improvement in mechanical strength was associated with the development of the elongated β–Si_3N_4 phase. Si_3N_4 gel casting foams based on these environmentally friendly gel formers presented a permeability level typical of those used in a wide variety of fluid flow and filtering applications.

CRediT author statement

E.G.M. designed the processing approach after discussion with P·C., prepared and characterized the samples, analyzed data, and wrote the original draft manuscript. M.D.M.I and L.B. performed permeability tests and contributed to the discussion of results and critical revision of the manuscript. A.P.N.O and D.H. contributed to the revision and editing of the manuscript. P.C. supervised and coordinate the research and participated in the revision and editing of the manuscript.

Declaration of interests

The authors declare that they have no known competing financial interests or personal relationships that could have appeared to influence the work reported in this paper.

Acknowledgments

Prof. H. Mandal of Sabanci University is gratefully acknowledged for providing silicon nitride powders. The authors gratefully acknowledge the support of the European Commission through the Marie-Curie ITN project “Functional Nitrides for Energy Applications, FUNEA” (FP7-PITN-GA2010-264873). E.G.M, A.P.N.O and D.H. would also like to thank the Coordenação de Aperfeiçoamento de Pessoal de Nível Superior - Brasil (CAPES) – CAPES-PRINT (Project Number: 88881.310728/2018-01).

References

[1] D.J. Green, P. Colombo, Cellular ceramics: intriguing structures, novel properties, and innovative applications, MRS Bull. 28 (4) (2003) 296–300.
[2] M. Scheffler, P. Colombo, Cellular Ceramics: Structure, Manufacturing, Properties and Application, Wiley-VCH, Weinheim, 2005.
[3] A.R. Studart, U.T. Gonzenbach, E. Tervoort, L.J. Gauckler, Processing routes to macroporous ceramics - a review, J. Am. Ceram. Soc. 89 (6) (2006) 1771–1789.
[4] P. Colombo, Conventional and novel processing methods for cellular ceramics, Phil Trans R Soc A 364 (1838) (2006) 109–124.
[5] P. Greil, Advanced engineering ceramics, Adv Mater 14 (10) (2002) 709–716.
[6] Schwartzwalder Karl, Arthur V. Somers, Method of making porous ceramic articles, U.S. Patent No. 3 (21 May 1963), 090,094.
[7] X. Pu, X. Liu, F. Qiu, L. Huang, Novel method to optimize the structure of reticulated porous ceramics, J. Am. Ceram. Soc. 87 (7) (2004) 1392–1394.
[8] A. Díaz, S. Hampshire, Characterisation of porous silicon nitride materials produced with starch, J. Eur. Ceram. Soc. 24 (2) (2004) 413–419.
[9] S. Barg, E.G. Moraes, D. Koch, G. Grathwohl, New cellular ceramics from high alkane phase emulsified suspensions (HAPES), J. Eur. Ceram. Soc. 29 (12) (2009) 2439–2446.
[10] H.X. Peng, Z. Fan, J.R.G. Evans, Busfield Jjc, Microstructure of ceramic foams, J. Eur. Ceram. Soc. 20 (7) (2000) 807–813.
[11] P. Sepulveda, J.G.P. Binner, Processing of cellular ceramics by foaming and *in situ* polymerisation of organic monomers, J. Eur. Ceram. Soc. 19 (12) (1999) 2059–2066.
[12] M. Potoczek, Gelcasting of alumina foams using agarose solutions, Ceram. Int. 34 (3) (2008) 661–667.
[13] J. Yang, J. Yu, Y. Huang, Recent developments in gelcasting of ceramics, J. Eur. Ceram. Soc. 31 (14) (2011) 2569–2591.
[14] M.I. Nieto, I. Santacruz, R. Moreno, Shaping of dense advanced ceramics and coatings by gelation of polysaccharides, Adv. Eng. Mater. 16 (6) (2014) 637–654.
[15] R. Moreno, Better ceramics through colloid chemistry, J. Eur. Ceram. Soc. 40 (3) (2020) 559–587.
[16] M.R. Nangrejo, X. Bao, M.J. Edirisinghe, Preparation of silicon carbide-silicon nitride composite foams from pre-ceramic polymers, J. Eur. Ceram. Soc. 20 (11) (2000) 1777–1785.
[17] J. Yu, J. Yang, H. Li, X. Xi, Y. Huang, Study of particle-stabilized Si3N4 ceramic foams, Mater. Lett. 65 (12) (2011) 1801–1804.
[18] E.G. Moraes, P. Colombo, Silicon nitride foams from emulsions, Mater. Lett. 128 (2014) 128–131.
[19] Y. Huang, L. Ma, Q. Tang, J. Yang, Z. Xie, X. Xu, Surface oxidation to improve water-based gelcasting of silicon nitride, J. Mater. Sci. 35 (14) (2000) 3519–3524.
[20] O. Lyckfeldt, J. Brandt, S. Lesca, Protein forming—a novel shaping technique for ceramics, J. Eur. Ceram. Soc. 20 (14) (2000) 2551–2559.
[21] G. Ziegler, J. Heinrich, G. Wötting, Relationships between processing, microstructure and properties of dense and reaction-bonded silicon nitride, J. Mater. Sci. 22 (9) (1987) 3041–3086.
[22] G. Ling, H. Yang, Pressureless sintering of silicon nitride with magnesia and yttria, Mater. Chem. Phys. 90 (1) (2005) 31–34.
[23] A.M. Alper, Phase Diagrams in Advanced Ceramics, Acad Press Ltd, London, 1995.
[24] H. Lange, G. Wötting, G. Winter, Silicon nitride-from powder synthesis to ceramic materials, Angew Chem Int Engl 30 (12) (1991) 1579–1597.
[25] X. Zhu, Y. Sakka, Textured silicon nitride: processing and anisotropic properties, Sci. Technol. Adv. Mater. 9 (3) (2008), 033001.
[26] R. Moreno, A. Salomoni, S.M. Castanho, Colloidal filtration of silicon nitride aqueous slips, part I: optimization of the slip parameters, J. Eur. Ceram. Soc. 18 (4) (1998) 405–416.
[27] C. Tuck, J.R.G. Evans, Porous ceramics prepared from aqueous foams, J. Mater. Sci. Lett. 18 (13) (1999) 1003–1005.
[28] E.G. Moraes, D. Li, P. Colombo, Z. Shen, Silicon nitride foams from emulsions sintered by rapid intense thermal radiation, J. Eur. Ceram. Soc. 35 (12) (2015) 3263–3272.
[29] A. Nagel, G. Petzow, P. Greil, Rheology of aqueous silicon nitride suspensions, J. Eur. Ceram. Soc. 5 (6) (1989) 371–378.
[30] C.R. Blanchard, S.T. Schwab, X-ray diffraction analysis of the pyrolytic conversion of perhydropolysilazane into silicon nitride, J. Am. Ceram. Soc. 77 (7) (1994) 1729–1739.
[31] H.X. Peng, Z. Fan, J.R.G. Evans, Busfield Jjc, Microstructure of ceramic foams, J. Eur. Ceram. Soc. 20 (7) (2000) 807–813.
[32] S. Barg, M.D. Innocentini, R.V. Meloni, W.S. Chacon, H. Wang, D. Koch, G. Grathwohl, Physical and high-temperature permeation features of double-layered cellular filtering membranes prepared via freeze casting of emulsified powder suspensions, J Memb Sci 383 (1–2) (2011) 35–43.
[33] M.D. Innocentini, W.S. Chacon, R.F. Caldato, G.R. Paula, G.L. Adabo, Microstructural, physical, and fluid dynamic assessment of spinel-based and phosphate-bonded investments for dental applications, Int J Appl Ceram Tec 12 (2) (2015) 306–318.
[34] A. Dey, N. Kayal, O. Chakrabarti, R. Caldato, C. Andre, M. Innocentini, V. Guerra, Studies on permeability properties and particle capture efficiencies of porous SiC ceramics processed by oxide bonding technique, in: 5th International Conference on Porous Media and Their Applications in Science, Engineering and Industry, Riverside, 2014.
[35] F.S. Ortega, P. Sepulveda, M.D.M. Innocentini, V.C. Pandolfelli, Surfactants: a necessity for producing porous ceramics, Am. Ceram. Soc. Bull. 80 (4) (2001) 37–42.
[36] M.D.M. Innocentini, R.K. Faleiros, J.R. Pisani, I. Thijs, J. Luyten, S. Mullens, Permeability of porous gelcast scaffolds for bone tissue engineering, J. Porous Mater. 17 (5) (2010) 615–627.
[37] L. Biasetto, P. Colombo, M.D.M. Innocentini, S. Mullens, Gas permeability of microcellular ceramic foams, Ind. Eng. Chem. Res. 46 (10) (2007) 3366–3372.
[38] S. Hampshire, K.H. Jack, Densification and transformation mechanisms in nitrogen ceramics, in: F.L. Riley (Ed.), Progress in Nitrogen Ceramics, Martinus Nijhoff publ, Lancaster, 1983, pp. 225–230.
[39] A. Pyzik, D. Beaman, Microstructure and properties of self-reinforced silicon nitride, J. Am. Ceram. Soc. 76 (11) (1993) 2737–2744.
[40] S. Bae, S. Baik, Critical concentration of MgO for the prevention of abnormal grain growth in alumina, J. Am. Ceram. Soc. 77 (10) (1994) 2499–2504.
[41] C.Y. Tan, A. Yaghoubi, S. Ramesh, S. Adzila, J. Purbolaksono, M.A. Hassan, M. G. Kutty, Sintering and mechanical properties of MgO-doped nanocrystalline hydroxyapatite, Ceram. Int. 39 (8) (2013) 8979–8983.
[42] E. Dickinson, Protein adsorption at liquid interfaces and the relationship to foam stability, in: A.J. Wilson (Ed.), Foams: Physics, Chemistry and Structure, Springer-Verlag, Heidelberg, 1989, pp. 39–53.
[43] D.C. Clark, M. Coke, L.J. Smith, D.R. Wilson, The formation and stabilisation of protein foams, in: A.J. Wilson (Ed.), Foams: Physics, Chemistry and Structure, Springer-Verlag, Heidelberg, 1989, pp. 55–68.
[44] O.R. Fennema, S. Damodaran, K.L. Parkin, Introduction to food chemistry, in: Fennema’s Food Chemistry, CRC Press, Boca Ratom, 2017, pp. 1–16.
[45] E. Dickinson, Hydrocolloids at interfaces and the influence on the properties of dispersed systems, Food hydrocoll 17 (1) (2003) 25–39.
[46] C. Wollenweber, A.V. Makievski, R. Miller, R. Daniels, Adsorption of hydroxypropyl methylcellulose at the liquid/liquid interface and the effect on emulsion stability, Colloids Surf., A 172 (1–3) (2000) 91–101.
[47] J.Y. Park, C.H. Kim, The α–to β–Si_3N_4 transformation in the presence of liquid silicon, J. Mater. Sci. 23 (9) (1988) 3049–3054.
[48] C. Zou, C. Zhang, B. Li, S. Wang, F. Cao, Microstructure and properties of porous silicon nitride ceramics prepared by gel-casting and gas pressure sintering, Mater. Des. 44 (1) (2013) 114–118.
[49] I. Nettleship, Applications of porous ceramics, Key Eng. Mater. 122 (1996) 305–324.
[50] L.J. Gibson, M.F. Ashby, Cellular Solids: Structure and Properties, second ed., Cambridge University Press, Cambridge, 1999.
[51] R. Brezny, D.J. Green, C.Q. Dam, Evaluation of strut strength in open-cell ceramics, J. Am. Ceram. Soc. 72 (6) (1989) 885–889.

[52] J.F. Yang, Z.Y. Deng, T. Ohji, Fabrication and characterisation of porous silicon nitride ceramics using Yb_2O_3 as sintering additive, J. Eur. Ceram. Soc. 23 (2) (2003) 371–378.
[53] M.D.M. Innocentini, P. Sepulveda, F.S. Ortega, Permeability, in: M. Scheffler, P. Colombo (Eds.), Cellular Ceramics: Structure, Manufacturing, Properties and Applications, Wiley-VCH, Weinheim, 2005, pp. 313–341.
[54] M.D.M. Innocentini, V.D. Rasteira, M. Potoczek, A. Chmielarz, E. Kocy'o, Physical, fluid dynamic and mechanical properties of alumina gel-cast foams manufactured using agarose or ovalbumin as gelling agents, J. Mater. Res. 32 (14) (2017) 2810–2818.
[55] C. Vakifahmetoglu, D. Zeydanli, M.D.M. Innocentini, F.S. Ribeiro, P.R.O. Lasso, G. D. Soraru, Gradient-hierarchic-aligned porosity SiOC ceramics, Sci. Rep. 7 (1) (2017) 1–12.